COVER PAGE

Final Report (DE-SC0008547)

Where Have All of the Electrons Gone? Understanding the Role of Alternative Electron Flow and O_2 Reduction in Balancing Cellular Redox

March 2nd 2021

OFFICE OF SCIENCE
Chemical Sciences, Geosciences, and Biosciences
Photosynthetic Systems and Physical Biosciences

Primary Institution – Point of Contact and Coordinator
Applicant/Institution: Colorado School of Mines
Street Address/City/State/Zip: 1500 Illinois Street, Golden, CO 80401
Principal Investigator (PI): Matthew C. Posewitz
PI Postal Address: Department of Chemistry and Geochemistry, Colorado School of Mines, 1500 Illinois Street, Golden, Colorado 80401
PI Telephone Number: 303-384-2425
PI email: mposewit@mines.edu

Funding Opportunity Announcement Number: DE-FOA-0001664

Administrative Point of Contact: Michele Land; 303-273-3405(office); mland@mines.edu

Topic Area: Photosynthetic systems

Collaborating Institution

Applicant/Institution: Carnegie Institute for Science (Arthur R. Grossman)
Street Address/City/State/Zip: 260 Panama Street, Stanford, CA 94305
Co-Principal Investigator (PI): Arthur R. Grossman
PI Postal Address: Carnegie Institute for Science, Department of Plant Biology, 260 Panama Street, Stanford, CA 94305
PI Telephone Number: 650-325-1521 x 212
PI Email: arthurg@stanford.edu

Abstract

An informed understanding of the fundamentals of light-driven electron transfer reactions in photoautotrophic organisms is necessary to enable improved photosynthetic efficiencies for the production of renewable fuels and novel biomaterials. To obtain high photosynthetic yields, light energy must be efficiently coupled to the fixation of CO_2. Sub-optimal environmental conditions and metabolic routing (caused by blocks in biosynthetic routes) can severely impact the conversion of light energy to biomass and lead to reactive oxygen production, which in turn can cause cellular damage and productivity losses. Hence, plants, algae, and photosynthetic bacteria have evolved a network of alternative outlets to sustain the flow of photosynthetically derived-electrons. Our research was focused on the nature and integration of these outlets. The data obtained in this project will inform efforts to rationally engineer crop plants and algae to improve photosynthetic yields by enhancing electron transfer reactions to CO_2 reduction and targeted biomass accumulation. A major project research thrust was focused on identifying and quantifying the flow of photosynthetic reductant through electron transfer circuits that result in the light-dependent reduction of O_2. New energy management strategies were identified that are used when normal carbon assimilation pathways are compromised due to nutrient deprivation, and/or by a reduction in starch synthesis/carbon storage, all conditions resulting in highly reduced intracellular redox pools. The green alga *Chlamydomonas reinhardtii*, and likely many other algae, have multiple O_2-reducing pathways that play critical roles in maintaining cellular metabolic balance and scavenging electrons that could potentially cause cellular damage, which in some instances leads to reduced photosynthetic yields but increased fitness. We explored the activities of three essential outlets associated with *Chlamydomonas reinhardtii* photosynthetic electron transport: (1) reduction of O_2 to H_2O through Flavodiiron proteins (FLVs) and (2) Plastid Terminal Oxidases (PTOX), and (3) the synthesis of starch. Real-time measurements of O_2 exchange demonstrated that FLVs immediately engage during dark to light transitions, allowing electron transport when the CBBC is not fully activated. Under these conditions, we quantified, for the first time, maximal FLV activity and its overall capacity to direct photosynthetic electrons towards O_2 reduction. However, when starch synthesis is compromised, a greater proportion of electrons is directed toward O_2 reduction through the FLVs, while PTOX, which is sensitive to the PQ pool redox state, is activated. This suggests, that starch synthesis has an important role in priming/regulating CBBC and electron transport. We also identified a biological 'switch' in the green alga *Chlamydomonas reinhardtii* that reversibly restricts photosynthetic electron transport (PET) at the cytochrome b_6f complex when reductant and ATP generated by PET are in excess of the capacity of carbon metabolism to utilize these products; we specifically show a restriction at this switch when *sta6* mutant cells, which cannot synthesize starch, are limited for nitrogen (growth inhibition) and subjected to a dark to light transition. This restriction causes diminished electron flow to PSI, which prevents PSI photodamage, and the plastid alternative oxidase (PTOX) becomes fully activated, serving as an electron valve that dissipates excitation energy absorbed by PSII, thereby lessening PSII photoinhibition. Furthermore, illumination of the cells following the dark acclimation gradually diminishes the restriction at the switch. Future engineering of these switches may allow more effective electron transfer to lipid (biofuel) pathways and diminish the number of electrons "wasted" in the reduction of O_2 to water. Lastly, we explored metabolic routing of electrons during algal fermentation and discovered multiple novel pathways that are activated when the preferred anoxic routes are blocked. These provide valuable products (e.g. lactate, glycerol) that can be used in broad portfolio of biotechnological applications.

Research Summary

Reversible switch regulates electron flow across cytochrome b_6f protecting PSI from photoinhibition

The fundamental research question on this project entailed dissecting the flow of electrons from water oxidation when two primary carbon sinks (starch and protein) are unavailable for the storage of fixed carbon. Currently, several biofuel efforts are focused on lipid synthesis, which could potentially be enhanced when protein and carbohydrate biosynthesis are blocked if photosynthesis remains active. Additionally, abiotic conditions on Earth, including temperature, light intensities, moisture and levels of available nutrients are rapidly being altered. Changing environmental conditions can constrain the growth and development of photosynthetic organisms and lead to an imbalance between the generation of energetic electrons by photosynthetic electron transport and the use of those electrons in the assimilation of CO_2 by the Calvin cycle and starch/lipid synthesis. When such imbalances occur, some of the solar energy absorbed by PSI and PSII can be converted to reactive oxygen species, which creates oxidative stress and consequently photoinhibition, degradation of photosynthetic reaction centers and damage to essential cellular components such as DNA, proteins and lipids. While an efficient system has evolved to repair damaged PSII, there is no corresponding system associated with PSI; recovery of PSI is slow or irreversible, which can strongly impact plant primary productivity. Hence, photosynthetic organisms have evolved mechanisms to dissipate excess absorbed light energy through nonphotochemical quenching and the use of shunts and alternative electron valves (not directly involved in CO_2 fixation) for photochemical quenching, many of which consume O_2 (**Figure 1**). The integration of these processes favor optimization of CO_2 fixation and assimilation, while at the same time protecting reaction centers from damage. In this project, we explored mechanisms by which Chlamydomonas protects PSI from photoinhibition when there is asymmetry between the rate of PET and the reduction and assimilation of inorganic C.

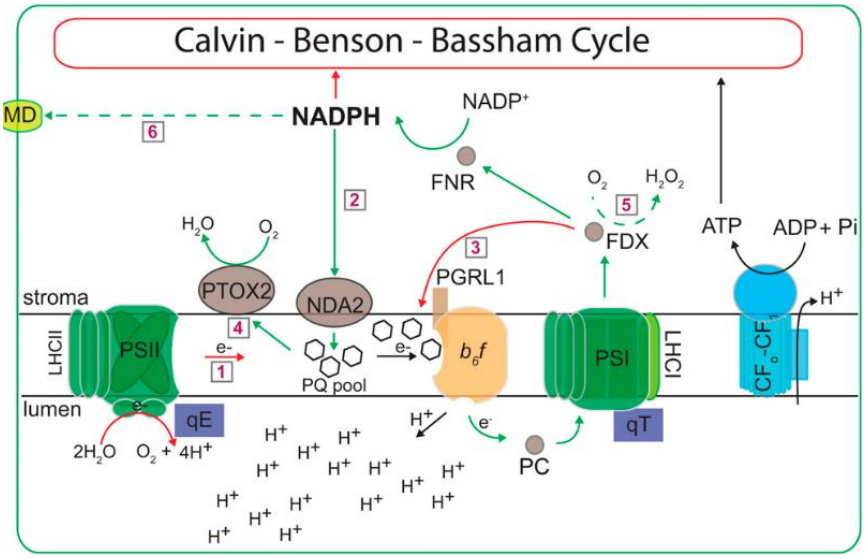

Figure 1. Dynamics of the photosynthetic machinery during photoautotrophic N deprivation. Electron flow pathways during N-deplete growth conditions are shown. Red arrows indicate processes that appear to be down-regulated (as well as the red circle around CBB), while green arrows indicate processes that appear to be up-regulated, during N deprivation (relative to nutrientreplete cells). Dashed green arrows represent pathways identified by others. Pathways are as follows: 1, LEF; 2, NDA2-dependent CEF; 3, PGR5/L1-dependent CEF; 4, chlororespiration; 5, Mehler reaction; 6, movement of reductant out of the chloroplast through the formation of malate by malate dehydrogenase (MD). FDX, Ferredoxin; FNR, ferredoxin NADP+ reductase; Pi, inorganic phosphate.

Chlamydomonas cells exposed to N deprivation undergo rapid metabolic acclimation in which light-generated reductant and ATP drive the assimilation of CO_2 into starch. It is not surprising, therefore, that a severe imbalance between PET and C assimilation occurs when the cells are both deprived of N and unable to synthesize starch, which is the case for *sta6*, especially during dark to light transitions (a condition in which the CBBC is not fully active due to redox control of the cycle. Consequently, the pool of available electron acceptors downstream of PSI would be severely limited, potentially leading to accumulation of ROS and irreversible photoinhibition of PSI.

A detailed analysis of electron transport in N-deprived *sta6* demonstrated that following dark acclimation there is a restriction in electron flow between the plastoquinone (PQ)-pool (or Q_o) and Cyt *f*. Accordingly, there is a marked reduction in the rate of quinol oxidation and diminished rates of linear electron flow. Importantly, the electron transport restriction in N-deprived *sta6* resulted in elevated P700 oxidization, a state in which PSI is photo-protected. Interestingly, the 'restricted state' could be reversed upon exposure of dark-acclimated, N-deprived *sta6* to light. Exposure of N-derived *sta6* cells to light allows photosynthetic electrons access to an alternate electron valve downstream of PSI.

Despite the restriction in electron transport at the Cyt b_6f complex, O_2 production in N-deprived *sta6* was not completely arrested. Real-time measurements of O_2 exchange demonstrated a maximal O_2 production rate of 20-25 µmol O_2 mg Chl^{-1} h^{-1} (this O_2 was consumed at approximately the same rate as it was generated; **Figure 2**), which is 4-5-fold slower than the rate of O_2 production by N-deprived C6 cells (~120 µmol O_2 mg Chl^{-1} h^{-1}; **Figure 2**). Based on the use of the inhibitor propyl gallate, the O_2 production and uptake (and electron transfer) in N-deprived *sta6* could be almost completely attributed to the function of a PTOX (plastid alternative oxidase) dependent H_2O-to-H_2O cycle (**Figure 2**). Importantly, the rates of O_2 production and uptake measured when photosynthetic electron transport was blocked were 5-6 e^- PSI^{-1} s^{-1} (conversions between O_2 production and electron transport rates were performed according to the ratio of 1 e^- PSI^{-1} $s^- \approx 4$ µmol O_2 mg Chl^{-1} h^{-1}), which matches the maximal rate of the PTOX reaction measured in Chlamydomonas, suggesting that PTOX is the main electron outlet in dark-acclimated, N-deprived *sta6*. We suggest that the photochemical quenching process mediated by PTOX is an essential component of photosynthetic control and may impact photosynthetic electron transport between PSII and PSI. The photochemical quenching activity of PTOX may not only contribute to protection of PSII, but may also generate a sufficient H^+ gradient (through the H_2O-to-H_2O cycle, which releases 2 H^+ on the lumenal side of the thylakoid membranes while taking up 2 H^+ on the stromal side) to enable ATP synthesis.

This research is currently in revision prior to publication and describes a biological 'switch' in the green alga *Chlamydomonas reinhardtii* that reversibly restricts photosynthetic electron transport (PET) at the cytochrome b_6f complex when reductant and ATP generated by PET are in excess of the capacity of carbon metabolism to utilize these products; we specifically show a restriction at this switch when *sta6* mutant cells, which cannot synthesize starch, are limited for nitrogen (growth inhibition) and subjected to a dark to light transition. This restriction causes diminished electron flow to PSI, which prevents PSI photodamage, and the plastid alternative oxidase (PTOX) becomes fully activated, serving as an electron valve that dissipates excitation energy absorbed by PSII, thereby lessening PSII photoinhibition. Furthermore, illumination of the cells following the dark acclimation gradually diminishes the restriction at the switch.

Elucidating this photoprotective mechanism, the modulating factors and the conditions associated with its activation offers new directions for optimizing photosynthesis.

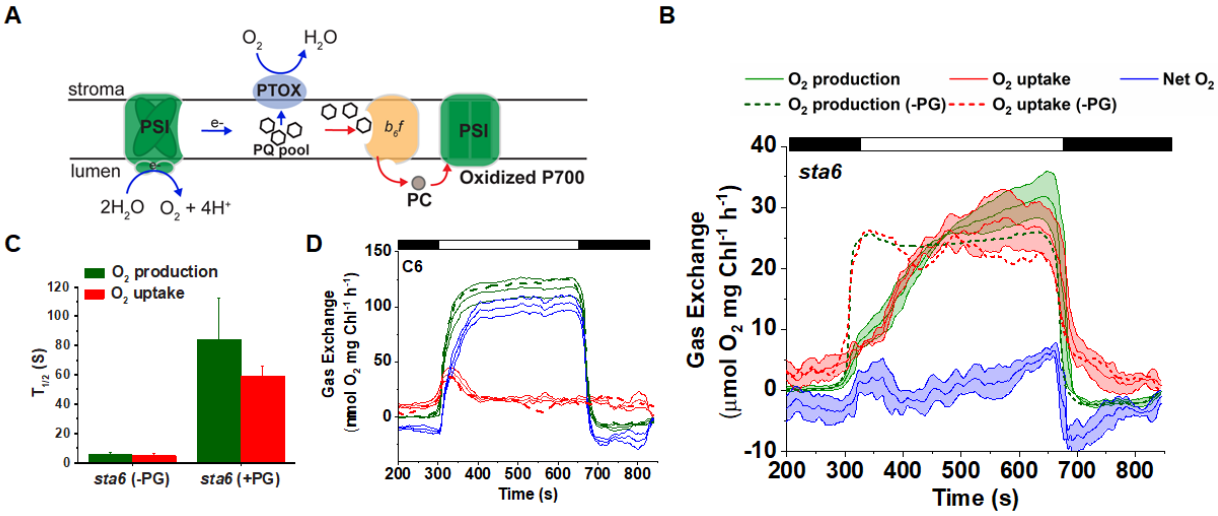

Figure 2: **Real time O_2 exchange for N-deprived cells in the presence of PTOX inhibitor: A.** Schematic of photosynthetic electron flow when electron flow across the Cyt *b_6f* complex is restricted in N-deprived *sta6*. Red and blue arrows indicate restricted and non-restricted pathways, respectively. **B.** Gross O_2 production ($^{16}O_2$ evolution, green curves) and gross O_2 uptake ($^{18}O_2$ consumption, red curves) are presented for N-deprived *sta6* both in the presence (solid curves) and absence (broken curves) of 2 mM propyl gallate (PG), an inhibitor of PTOX. Net O_2 production in the presence of PG is shown by the blue curves. Experimental design was as in **Figure 2**. Each curve represents an average of at least 3 biological replicates ± SE. **C.** $T_{1/2}$ for attaining Pmax (green bars) and Umax (red bars) in N-deprived *sta6* in the presence and absence of PG. Rates were calculated after fitting the O_2 production and uptake curves to a first order exponential decay. The presented data is an average of at least 3 biological replicates ± SD. **D.** Gross O_2 production ($^{16}O_2$ evolution, green curves) and gross O_2 uptake ($^{18}O_2$ consumption, red curves) are presented for N-deprived C6 both in the presence (solid curves) and absence (broken curves) of 2 mM propyl gallate (PG). Net O_2 production in the presence of PG is shown by the blue curve. Experimental design was as in **Figure 2**. Each curve represents an average of at least 3 biological replicates ± SE.

Alternative outlets for sustaining photosynthetic electron transport during dark to light transitions

Saroussi, S., Karns, D.A.J., Thomas, D.C., Bloszies, C., Fiehn, O., **Posewitz, M.C.** and Grossman, A.R. (2019) Alternative outlets for sustaining photosynthetic electron transport during dark to light transitions. *Proceedings National Academy of Sciences*, **116**, 11518-11527.

Environmental stresses dramatically impact the balance between production of photosynthetically-derived electrons and the activity of the Calvin-Benson-Bassham Cycle (CBBC); an imbalance promotes accumulation of reactive oxygen species and cause cell damage. Hence, photosynthetic organisms have developed several strategies to avoid photo-damage by routing electrons towards alternative outlets. In this work, we explore the activities of three essential outlets associated with *Chlamydomonas reinhardtii* photosynthetic electron transport: (1) reduction of O_2 to H_2O through Flavodiiron proteins (FLVs) and (2) Plastid Terminal Oxidases (PTOX), and (3) the synthesis of starch. Real-time measurements of O_2 exchange have demonstrated that FLVs immediately engage during dark to light transitions, allowing electron transport when the CBBC is not fully activated. Under these conditions, we quantified, for the first time, maximal FLV activity and its overall capacity to direct photosynthetic electrons towards O_2 reduction. However, when starch synthesis is compromised, a greater proportion of electrons is directed toward O_2 reduction through the FLVs, while PTOX, which is sensitive to the PQ pool redox state, is activated. This suggests, that starch synthesis has an important role in priming/regulating CBBC and electron transport. Moreover, switching the circuitry of light-driven electrons between sustainable (starch; electrons can be recaptured) and non-sustainable (H_2O; electrons cannot be recaptured) outlets are part of energetic management that allows photosynthetic organisms to cope with frequent environmental fluctuations encountered in nature. Lastly, unmasking the repertoire of such energetic reactions reveals new directions for rational re-design and optimization of photosynthesis to satisfy global demands for food, biofuels and other resources.

Starch synthesis, a sink for reductant/fixed carbon and ATP, can potentially impact which of the various cellular pathways are used to consume photosynthetically-derived electrons. In the absence of starch synthesis, the excess excitation that cannot be coupled to downstream C metabolism could potentially be nonphotochemically quenched and/or the excited electrons may be photochemically quenched through activation of alternative pathways that deliver photosynthetically-derived electrons to O_2 to generate H_2O; these pathways result in O_2 uptake. Furthermore, at the onset of a dark to light transition, the reactions involved in fixing CO_2 (CBBC) are not fully active and therefore are not optimally integrated with photosynthetic electron transport. To explore the extent of photochemical processes associated with quenching of excess excitation and how these processes are integrated with photosynthetic C metabolism, we monitored the dynamics of O_2 evolution and uptake during dark to light transitions in the *sta6* starchless mutant. As a control for this analysis, we used the genetically complemented (*sta6*::STA6) C6 strain.

Membrane Inlet Mass Spectrometry (MIMS) was used to quantify O_2 production ($^{16}O_2$ evolution) and uptake (depletion of injected $^{18}O_2$ from the medium) upon exposure of *sta6* and C6 cells to increasing light intensities (50, 150, 300 and 1000 μmol photons m^{-2} s^{-1}) during photoautotrophic growth in the presence of elevated CO_2 (**Figure 1**). The trends for O_2 production and uptake changed to some extent over the time of the light treatment (at any

intensity used), we therefore divided the light period (6 min in total, represented by white bars above graph in **Figure 1**) into an early phase (first 3 min) and late phase (last 3 min).

When C6 cells were exposed to light after a 5 min dark preincubation, the rate of gross $^{16}O_2$ production rapidly increased to a maximal rate, or Pmax, and remained steady for the remainder of the light treatment (green curve, **Figure 1A**). Pmax was positively correlated with an increase in light intensity and attained a maximum value of ~190 µmol O_2 mg^{-1} Chl h^{-1} at 1000 µmol photon m^{-2} s^{-1} (**Figures 1A** and **2A**). We also measured O_2 uptake by C6 cells, which exhibited a pronounced peak (Umax; maximum O_2 uptake rate) at the onset of the light (red curve **Figure 1A**). The Umax, like the Pmax, was positively correlated with light intensity, attaining a rate of ~80 µmol O_2 mg^{-1} Chl h^{-1} at 1000 µmol photon m^{-2} s^{-1} during the early phase of the light period (**Figure 1A** and **Figure 2A**). The ratio of Umax to Pmax (Umax/Pmax), which reflects the fraction of reductant generated by the photosynthetic light reactions that is not coupled to CO_2 fixation/metabolism or nutrient assimilation (e.g. reduction of nitrite or sulfate), did not markedly vary at the different light intensities tested during the early phase of the light exposure (~0.4). It did, however, decline during the later stages of light exposure, and appeared to stabilize at ~0.25 (**Figure 2A**). Consequently, for C6, the rise in net O_2 production with increasing light intensity (blue curve, **Figure 1A**) lagged relative to the initial rise in gross O_2 production (green curve, **Figure 1A**). At all light intensities, immediately following the Umax peak, the net production of O_2 rose to its maximal value, or $Pmax_{net}$ ($Pmax_{net}$ values were correlated with light intensity as well, **Figure 2A**).

Surprisingly, O_2 production and uptake by *sta6* cells showed trends that were notably different from those of C6 (**Figure 1B**). The mutant cells exhibited a burst of gross O_2 production (green curve, **Figure 1B**) soon after they were transferred from darkness to light, followed by a gradual decline to a steady state level of O_2 evolution. Similar to the C6 cells, Pmax was positively correlated with light intensity, although levels of gross O_2 evolution were almost 2-fold lower than the levels observed for C6 (**Figure 1** and **2B**). Simultaneous with the burst in O_2 production, the rate of O_2 uptake began to increase (at 150 µmol photons m^{-2} s^{-1} and above), reaching Umax soon after the burst of gross O_2 production (red curve, **Figure 1B**). Although the Umax for *sta6* and C6 were similar during the early phase of the light period (compare **Figures 2A** and **2B**), the uptake of O_2 slowly declined in *sta6* over a longer period than the decay of O_2 uptake in C6 cells (compare red curves in **Figures 1A** and **1B**). Furthermore, the Umax/Pmax value for *sta6* cells was ~0.8 during the early phase of the light period, resulting in a low rate of net O_2 production (**Figure 2B**). These results suggest that a smaller proportion of reductant generated by PSII in *sta6* was coupled to CO_2 fixation (or nonoxygen related reduction reactions) relative to C6. The Umax/Pmax for *sta6* decreased during the late phase of the light period (0.5-0.6; **Figure 2B**), suggesting reduced activity of pathways that use O_2 as a terminal acceptor of electrons relative to those in which the terminal acceptor is not O_2.

Taken together, these O_2 exchange analyses for C6 and *sta6* suggest that a defect in starch biosynthesis and the consequent loss of an outlet for electrons/fixed C and ATP resulted in a greater proportion of the light-generated electrons being directed toward outlets that involve O_2 reduction. Furthermore, a peak in light-dependent O_2 uptake in C6 occurred soon after the cells were exposed to light and prior to a rise in net light-dependent O_2 production. This O_2 uptake likely reflects FLV protein activity, which has been shown to engage immediately after the onset of light. Importantly, *sta6* cells exhibited a unique $^{18}O_2$ uptake pattern reflected by a broader peak (lasting a few min) than in C6. This suggests that the activity of the FLV proteins is more

sustained in the mutant and/or that more than one component may contribute to photoreduction of O_2.

To further elucidate the nature of light-dependent O_2 uptake and potential participation of alternative electron outlets during the transition from dark to light, we analyzed the kinetics of O_2 production and uptake for C6 and *sta6* cells in more detail (**Figure 3**; cells were exposed to 300 μmol photons m^{-2} s^{-1}). Although the rate of gross O_2 production was lower in *sta6* than in C6 (**Figures 1** and **2**), the kinetics of the initial rise of gross O_2 production over the first 20 s of the light period was similar between the strains (linear fitting of the initial rise of $^{16}O_2$ production; slopes are 4.5 and 4.1 for C6 and *sta6*, respectively; **Figure 3A,** dashed-dotted curves). Furthermore, during this period, the two strains exhibited similar kinetics for the rise in $^{18}O_2$ uptake (the rise in O_2 uptake was fitted to a first-order exponential decay type curve and gave values $\tau = 2.4$ s^{-1} and 2.0 s^{-1} for C6 and *sta6*, respectively**;** t-test, *p-value =0.23*; **Figure 3A**), suggesting that a similar mechanism may be involved in eliciting the initial light-driven production and uptake of O_2 for the two strains. However, while $^{18}O_2$ uptake for C6 cells decayed to a basal level soon after Umax was attained, the rate of O_2 uptake in *sta6* cells remained constant for at least 100 s followed by a slowl decay (**Figure 3A**, **inset**). Overall, *sta6* cells showed a 3-fold slower decay rate than C6 cells (slopes are -0.15 and -0.46, for C6 and *sta6*, respectively; $^{18}O_2$ uptake curves for a longer period of time are shown in the inset of **Figure 3A**). These observations demonstrate that the starchless mutant directed a greater proportion of electrons to photochemistry associated with the uptake of O_2 over the entire light period relative to the complemented strain.

We also observed this phenomenon when we compared the ratio of gross uptake and production of O_2 in C6 and *sta6* cells (**Figure 3B**). Immediately after the cells were exposed to light, the ratio of O_2 uptake to production was over 0.9 for both strains. After 20-30 s in the light, this ratio similarly declined to ~0.6 (as a result of a similar increase in gross O_2 production; highlighted in gray box) in both C6 and *sta6* cells. However, while this ratio continued to fall to ~0.1 for C6 cells, the proportion of O_2 uptake to production for *sta6* increased to ~0.8 after 100 s and remained much higher than that of C6 cells along the entire 6 min light period (**Figure 3B**). Comparable trends were found when the cells were exposed to lower or higher light intensities (50, 150 and 1000 μmol photons m^{-2} s^{-1}).

In sum, immediately following exposure to light, the CBBC is not fully activated and the high energy electrons generated by photosynthetic electron transport cannot immediately be used for CO_2 fixation. Under such circumstances, the cells, regardless of whether they have the capacity to store C as starch, share a common electron outlet, the FLV proteins (as mentioned in the above paragraph) that sustain PSII O_2 production with the concomitant reduction of O_2 to H_2O. Moreover, the altered kinetics of O_2 uptake and decay in *sta6* (slower decay of $^{18}O_2$ uptake and a much higher $^{18}O_2$ uptake/$^{16}O_2$ evolution ratio during much of the light period) suggest that as compensation for the loss of starch synthesis, i.e. in *sta6* cells, the reduction of O_2 in *sta6* is more dominant than in C6 and support the possibility that there is more than one component contributing to O_2 uptake during the light period. These results raise the possibility that activation of the CBBC (or downstream reactions) is slower in the mutant than in the complemented cells which results in an increased contribution of FLV to the reduction of O_2 and H^+ (the CBBC and FLV compete for the same pool of electrons). Alternatively, slower activation of CBBC and consequently a decrease in the pool of downstream electron acceptors resulting from the loss of starch synthesis in *sta6* feeds back on electron transport causing hyper-reduction of the PQ pool, which in turn may activate PTOX and result in increased O_2 consumption.

Lastly, we cannot rule out the possibility that mitochondrial respiration becomes a more dominant contributor to total $^{18}O_2$ uptake in *sta6*. This last possibility seems less likely since the O_2 uptake rate measured in the dark (immediately following the light to dark transition) is slower in *sta6* than in C6.

To further probe potential contributions of FLVs and assess the role of PTOX in routing electrons during a transition from darkness to light, we supplemented cultures with 2 mM propyl gallate (PG), a reagent that inhibits alternative oxidases such as PTOX but does not inhibit FLV activity. This inhibitor was added to cultures at the beginning of the dark period (5 min prior to light exposure) and its impacts on O_2 production and uptake were monitored during the light (300 µmol photos m^{-2} s^{-1}) period. PG did not affect the overall trends of O_2 production and uptake in C6 cells, however, the Pmax (both net and gross) was ~60% of the value measured in the absence of PG (**Figure 4A** and **Table 1**). In contrast, in PG-treated *sta6* cells the initial burst of gross $^{16}O_2$ production was completely suppressed and Pmax was 46% of that of untreated *sta6* cells (**Figure 4B** and **Table 1**), resulting in a similar rate of $^{18}O_2$ uptake and $^{16}O_2$ production and a net O_2 production of zero (**Figure 4B**). As the length of exposure to the light increased, $^{18}O_2$ uptake slightly declined while both net and gross $^{16}O_2$ evolution gradually rose (**Figure 4B**).

Umax of both untreated and PG-treated C6 cells was attained at approximately the same time following exposure to light, but the Umax value of PG-treated C6 cells was ~68% of that of untreated cells (**Figure 4C** and **Table 1**, Umax for untreated and treated cells are indicated with a solid and dashed red line extended from the x-axis, respectively) and the rate at which Umax was attained was slower by more than 2-fold (initial slopes of 1.9 and 4.4 for PG-treated and untreated C6, respectively; **Figure 4C**). For *sta6*, untreated cells attained Umax 15 s faster than for PG-treated cells. The Umax value of PG-treated cells was ~60% of that of untreated cells (**Figure 4D** and **Table 1**, Umax for untreated and treated cells are indicated with a solid and dashed red line, respectively, extended from the x-axis) and the rate at which the Umax was attained was slower by ~3.5-fold (**Figure 4D**, initial slopes of 0.9 and 3.2 for PG-treated and untreated *sta6* cells, respectively). However, the overall trend of $^{18}O_2$ uptake in *sta6* cells following the initial rise was not markedly impacted; the rate of O_2 uptake stayed constant for an initial period of ~100 s in the light and then gradually slowed, but high values of Umax/Pmax were maintained over the entire light period (**Figures 4B, 4D** and **Table 1**).

Since PTOX modulates the redox state of the PQ pool, its inhibition by PG prior to the light period could limit oxidation of the quinol pool (in the dark), which would lead to a decline in the rates of both light-driven O_2 production and uptake, a lower Pmax, and a slower rise in the uptake of O_2, as shown in **Figures 4C** and **D**. To explore this possibility, we measured the redox state of the PQ pool, as 1-qL, after exposing PG-treated and untreated cells to 300 µmol photons m^{-2} s^{-1} for 1 min. For untreated cells, the PQ pool was 30% more reduced in *sta6* than in C6 (1-qL value was 0.63 ± 0.01 and 0.49 ± 0.06, respectively; **Figure 4E**), reflecting the feedback on electron transport as a consequence of compromised starch synthesis. Upon PG treatment, the reduction state of the PQ pool of both C6 and *sta6* increased by ~25%, but it was more reduced in *sta6* than in C6 cells (0.83 ± 0.00 and 0.61 ± 0.06, respectively; **Figure 4E**). These findings suggest that slower rates of O_2 production could be a consequence of elevated reduction of the PQ pool resulting from PTOX inhibition, however, the impact of this inhibition is much more pronounced in *sta6* cells. Furthermore, when we measured the redox state of the PQ pool as a function of increased light intensity, we found that C6 cells treated with PG maintained a redox state close to that of untreated cells (**Figure 4F**, triangles). Hence, PTOX appears to have a minor impact on total light-driven uptake of O_2 when starch metabolism is not impaired (i.e. in

C6 cells) but is important when the cells are maintained in the dark. In contrast, the PQ pool of PG-treated *sta6* cells was more reduced than the non-treated cells at all light intensities (**Figure 4F**, circles), but especially at low/moderate intensities, suggesting that the PG treated *sta6* cells are compromised in their ability to oxidize the PQ pool, likely a consequence of an additive effect of PTOX inhibition and an inability to synthesize starch in the light. Together, these experiments suggest that PTOX is essential for balancing the redox state of the PQ pool when the cells are maintained in the dark. Eliminating PTOX activity slows the rate of O_2 production upon shifting the cells to the light regardless of whether the cells can synthesize starch. Moreover, the finding that PG-treated *sta6* cannot maintain the redox state of the PQ pool (unlike PG-treated C6; **Figure 4F**) suggests that the loss of starch synthesis eliminates an important electron outlet that may elicit feedback inhibition of CBBC and/or electron transport, which leads to an increase in excitation pressure on the PQ pool.

To further explore the role of starch synthesis as an alternative outlet for C, we analyzed the levels of phosphorylated sugar intermediate focusing on the conversion of F6P to CBBC related metabolites (Xylulose-5-phospahate, X5P, and Ribulose-5-phosphate, R5P, metabolites in the pathway leading to the regeneration of Ribulose-1,5-bisphosphate, RuBP) and metabolites associated with gluconeogenesis and starch synthesis (G6P and Glucose-1-phosphate, G1P) at different time points along the transition from darkness to light (300 µmol photons m^{-2} s^{-1}, **Figures 6)**. Within the first 60 s in the light (the time in which O_2 uptake started to decline after reaching its peak (**Figure 3A**)), the levels of F6P increased by almost 4-fold relative to that of dark acclimated cells. Furthermore, the levels of G6P and G1P, increased by about 5 and 2.5-fold, respectively. In contrast, the levels of X5P, and R5P, did not vary much from the values measured in the dark. A similar trend was detected when we repeated the experiment with *sta6* cells (**Figures 5**); the levels of G6P and G1P increased by more than 3 and 2-fold relative to the dark acclimated state while the levels of X5P and R5P did not changes. However, the concentration of G6P and G1P measured for *sta6* cells was much lower than that of the C6 cells (G6P: 28.60 ± 2.47 and 7.7 ± 0.4 ng/10^6 cells; G1P: 169.54 ± 8.99 and 59.4 ± 6.7 ng/10^6 cells, C6 and *sta6* respectively, **Figure 5**), possibly indicating that starch synthesis has a regulatory role on CBBC enzyme activity. Lastly, since *sta6* cannot synthesize starch, the levels of G6P and G1P keep increasing after two min in the light while they decline somewhat in C6 cells. Taken together, these results indicate that there is an increase flow of C toward starch biosynthesis soon after the dark acclimated cells are exposed to light.

In prior work, it was shown that the FLV proteins are prominent outlets for electrons when the light is first turned on and photosynthetic electron transport is not optimally integrated with downstream C metabolism. Moreover, in C6 cells, where starch biosynthesis is normal, we observed a burst of O_2 uptake and a change in the PQ redox state during the dark to light transition that was little impacted when PTOX was inhibited (**Figure 4F**). Therefore, FLV is likely the dominant activity responsible for the O_2 uptake in C6. hence, we sought to quantitatively evaluate the role of the FLV proteins in reduction of O_2 during the dark to light transition. To quantify the contribution of FLV activity to O_2 uptake, we calculated the basal rate of light-driven O_2 uptake using a linear fit of the $^{18}O_2$ uptake data at steady state at various light intensities (late phase of light period), shown in **Figure 1A**. This uptake rate was correlated with uptake resulting from dark respiration based on O_2 electrode measurements. **Figure 6A** presents the overall O_2 uptake for C6 cells exposed to four different light intensities (solid lines, 50, 150, 300 and 1000 µmol photons m^{-2} s^{-1}). Also shown are the calculated basal rates of O_2 uptake (which is probably dominated by mitochondrial respiration) at the different light intensities

(horizontal dashed lines with the same colors as curves for $^{18}O_2$ uptake). By integrating the area under the O_2 uptake curve, using a baseline value established for the basal O_2 uptake at each of the four light intensities, we calculated the total amount of consumed O_2 that is associated with shifting the cells from dark to light and potentially a consequence of FLV. The amount of O_2 consumed by putative FLV activity increased with increasing light intensity. At 300 μmol photons m^{-2} s^{-1}, the FLV proteins consumed 0.46 ± 0.04 μmol O_2 mg Chl^{-1}, with maximum consumption at 1000 μmol photons m^{-2} s^{-1} (0.682 ± 0.16 μmol O_2 mg Chl^{-1}; **Figure 6B**). Interestingly, the maximal rate of O_2 uptake (Vmax) that we attributed to FLV activity was 45.7 ± 4.2 μmol O_2 mg Chl^{-1} h^{-1} when the cells were exposed to 300 μmol photons m^{-2} s^{-1}. This rate is not significantly different from the rates measured for cells exposed to 150 or 1000 μmol photons m^{-2} s^{-1} (**Figure 6C**). Therefore, while FLV proteins operate at Vmax, even upon exposure to moderate light intensities, the amount of O_2 consumed following the transfer of the cells to increasing intensities of light appears to be a consequence of prolonged activation of the FLV (more sustained uptake at higher light intensities).

Table 1: Photosynthetic parameters of PG treated C6 and *sta6* cells at 300 µmol photons m^{-2} s^{-1}. O_2 gas exchange (Pmax, Umax and Net O_2 evolution) presented as µmol O_2 mg Chl^{-1} h^{-1}

C6

	Early					Late				
Photosynthetic parameter	**PG+**	**SD**	**PG-**	**SD**	**PG+/PG- x100**	**PG+**	**SD**	**PG-**	**SD**	**PG+/PG- x100**
Pmax	100.5	10.8	164.4	1.0	61.2	103.0	13.6	166.7	4.6	61.7
Umax	46.5	7.0	67.6	3.6	68.8	25.4	0.8	42.0	10.0	60.3
Umax/pmax x 100	46.3	11.7	41.1	2.5	114.5	26.7	4.6	25.3	6.8	98.4
Net	91.4	10.9	153.3	0.4	59.7	98.3	15.9	165.9	1.9	59.2

sta6

	Early					Late				
Photosynthetic parameter	**PG+**	**SD**	**PG-**	**SD**	**PG+/PG- x 100**	**PG+**	**SD**	**PG-**	**SD**	**PG+/PG- x 100**
Pmax	46.0	4.9	99.7	6.7	46.1	52.5	4.1	75.1	5.8	69.9
Umax	42.9	7.8	71.7	5.6	59.8	36.7	9.4	42.1	8.0	87.3
Umax/pmax x 100	93.2	0.3	72.0	4.8	129.0	77.3	9.3	55.7	6.8	124.4
Net	26.8	7.1	45.9	8.2	67.4	37.7	7.5	47.9	5.0	78.7

In nature, photosynthetic organisms are frequently exposed to abiotic stresses, including marked variations in temperature and light intensities and suboptimal nutrient concentrations. Such environmental restrictions limit the growth/development of organisms and dramatically impact the use of photosynthetically-generated electrons for CO_2 fixation. To cope with environmental challenges, photosynthetic organisms have developed several strategies to manage excitation energy and reroute electrons to alternative pathways. To uncover the nature of various alternative pathways for electron flow and the flexibility of the energetic circuitry, we adopted an integrated approach to analyze the dynamics associated with photoreduction of O_2 through FLV and PTOX activities and photosynthetic C metabolism, including starch synthesis, during dark to light transitions, a condition under which photosynthetic electron transport and C metabolism are not in equilibrium. The *sta6* mutant, which is unable to synthesize starch, was used to evaluate how the flow of C toward starch impacts electron flow during the dark to light transition.

Elimination of starch synthesis in Chlamydomonas resulted in a pronounced decrease in light-dependent O_2 evolution (**Figures 1** and **2**), suggesting interactions between photosynthetic electron transport and downstream processes that consume electrons. Real-time analyses of gross O_2 exchange using isotopically labeled O_2 to distinguish between production ($^{16}O_2$) and light-driven uptake ($^{18}O_2$) demonstrated that *sta6* cells exhibited more sustained light-induced reduction of O_2 that was as high as 80% of the gross O_2 evolution (compared to 20-40% for C6 cells), and consequently the cells had low net O_2 evolution (**Figures 1**, **2** and **3B**). The lower maximal $^{16}O_2$ production and the elevated ratio of O_2 uptake to production (reflecting the fraction of reductant not used for CO_2 fixation and growth) highlights an essential role for starch synthesis as a transient outlet for storing reductant/energy generated by photosynthetic electron transport as the cells are activating downstream C metabolism. Furthermore, despite the lower rates of gross O_2 production exhibited by *sta6* relative to C6 cells, we did not observe a dramatic decrease in electron flow through PSII (measured as ΦPSII) when the cells were exposed to light intensities as high as 300 μmol photons m^{-2} s^{-1}. This discrepancy may be explained by activation of cyclic electron flow around PSII (PSII-CEF). Although this type of alternative pathway has not been intensively investigated, several studies suggest that PSII-CEF is activated under conditions in which the PQ pool is highly reduced. A potential role for PSII-CEF in *sta6* cells requires additional investigation.

Genes encoding FLV proteins are present in prokaryotes, green alga, moss, liverwort, lycophytes, and gymnosperms but are not found in vascular plants. These proteins function as an outlet for electrons when C metabolism is not optimally coupled to the rate of photosynthetic electron flow. Our analyses revealed a rapid increase in light-driven reduction of O_2 that takes place soon after Chlamydomonas cells are transitioned from the dark to the light. The kinetics of this 'burst' of O_2 uptake was similar for C6 and *sta6* (~2.4 s^{-1} at 300 μmol photons m^{-2} s^{-1}; **Figure 3A**) and is consistent with a function of FLVs in priming photosynthetic electron transport and harmlessly dissipating electrons prior to the activation of the CBBC and downstream C metabolism. In this context, recent work has demonstrated that slowed electron transport in Arabidopsis resulting from a defect in CEF (*pgr5* mutant, associated with CEF control) could be reversed by transforming the mutant plants with the *FLV* genes. Similarly, a Chlamydomonas *pgr5* mutant accumulates FLVs when the cells are exposed to HL. In these two examples, FLVs provide an alternative route for an 'overflow' of electrons (more electrons produced by the light reactions than can be used by downstream anabolic processes) by redirecting them toward the reduction of O_2 to generate H_2O. Importantly, our analyses allowed us, for the first time, to estimate the energy loss through dissipation of electrons by FLV-

mediated photoreduction during the dark to light transition and the maximum rate of electron flow from FLV to O_2. C6 cells shifted from dark to light revealed a Vmax for O_2 uptake by FLV of ~45 μmol O_2 mg Chl^{-1} h^{-1} under the conditions of our study (**Figure 6C**), which is equivalent to 22.5 e^- s^{-1} PSI^{-1} (conversion between units was done according to. A threshold for Vmax could limit the capacity of electron dissipation under conditions of high photon flux. We therefore also measured the total O_2 uptake by the FLV proteins at different light intensities, (**Figure 6A**). Based on our calculations, the total amount of O_2 consumption associated with the dark to light burst increased as a function of light intensity (ranging from 0.15 to 0.7 μmol O_2 mg Chl^{-1} for C6; **Figure 6B**). This increased photochemical dissipation is reflected by a broadening of the O_2 uptake peak that resulted because of a slower decay in O_2 uptake (**Figure 6A**). This slowed decay may be part of a compensation mechanism that diverts electrons to FLV when the redox pressure on the CBBC and perhaps downstream C utilization processes increase because these pathways are not yet fully activated.

While FLVs maintain photosynthetic electron transport generated by PSII during the transition from dark to light through reduction of O_2, C-intermediates rapidly flow towards starch synthesis as indicated by an increase in the concentration of G6P and G1P after 60 s following dark to light transitions (**Figures 5**). In contrast, there was little change in the levels of X5P and R5P over a 5 min exposure of the cells to light. The buildup of G6P and G1P in C6 cells aligned with the decrease of the initial O_2 uptake burst (**Figure 3A**) and is congruent with the time needed for redox activation of FBPase, and the slightly slower activation of PKR (catalyzes conversion of R5P to RuBP). In *sta6* cells the concentrations of phosphorylated sugar intermediates were much lower than in the C6 complemented line (**Figure 6** and **Table S1**). We therefore raise the possibility that the starch metabolic pathway has a regulatory effect on CBBC enzymes which explains the strain's low gross O_2 production (**Figures 2B** and **3**), not only in Chlamydomonas but also in Arabidopsis. Further analyses are required to describe the mechanism underlying this regulatory effect. Based on these findings, we propose that the starch biosynthesis pathway is activated soon after the light is switched on and drains C metabolites out of the CBBC to prevent feedback inhibition on CBBC's enzymes while they are not fully active; hence this pathway can maintain the activity of CBBC and sustain photosynthetic electron transport.

Other electron valves may also play a role in sustaining nondestructive electron transport during dark to light transitions. PTOX oxidizes quinol molecules downstream of PSII and is required for adjusting the redox balance of the PQ pool. The rate of quinol oxidation by PTOX was found to be relatively slow, only 5 e^- s^{-1} PSI^{-1} in Chlamydomonas, ~4-fold slower than the rate of NADPH oxidation by FLVs (as calculated in this study). However, it was shown that stressed organisms that experience a highly reduced PQ pool accumulate high levels of PTOX proteins, which would facilitate PTOX-dependent reduction of O_2 to H_2O. Here we show that PTOX may have a minor contribution to overall O_2 uptake when C6 cells (i.e. normal starch biosynthesis) are shifted from darkness to 300 μmol photons m^{-2} s^{-1} (**Figure 5**). Nevertheless, inactivation of PTOX using PG led to an elevated reduction of the PQ pool for both C6 and *sta6* when the cells were maintained in the dark (**Figure 5E**), which highlights the importance of PTOX in regulating the redox state of the PQ pool in darkness. On the other hand, when starch synthesis was compromised (i.e. in *sta6* cells), the redox state of the PQ pool was highly elevated at all light intensities (**Figure 4F**). Hence, we suggest that PTOX can become an important alternative outlet for electrons when various aspects of C metabolism/utilization, such as the storage of electrons in starch, are depressed.

Re-routing of electrons through alternative outlets allows photosynthetic organisms to cope with fluctuating environmental conditions. Here we show that Chlamydomonas activates various 'sustainable' and 'non-sustainable' electron transport pathways. The transient storage of fixed C such as starch represents a sustainable sink for excitation energy; the energy is not lost but can be deployed for growth and maintenance when needed. However, under conditions in which CO_2 fixation and C storage are compromised and/or saturated, the cells can photochemically quench absorbed excitation energy through photoreduction of O_2, a non-sustainable outlet (the energetic electron can no longer be used as a source of energy) in which photosynthetically-generated electrons are used for the catalytic reduction of O_2 to H_2O; FLV and PTOX can both catalyze this reaction. While photosynthetic reaction centers and electron transport components provide reducing equivalents that fuel C metabolism, FLVs appear to function as a clutch, dissipating excess energy stored in the electron transport system when the CBBC has not been fully 'switched on', suggesting potential regulatory interactions between CBBC proteins/metabolites and FLV activity. On the other hand, synthesis of starch acts as a battery that is being charged and prevents feedback inhibition of CBBC's enzyme by phosphorylated CBBC sugars; the energy stored as starch can be used when needed through catabolic reactions that release reductant, ATP and C backbones. Lastly, PTOX proteins are sensitive to redox changes associated with the PQ pool, which can be triggered by limitations in electron utilization by downstream reactions. As the redox state of the photosynthetic electron transport chain increases and a greater proportion of the PQ pool becomes reduced, PTOX acts like a valve on a pressure cooker, facilitating routing of 'overflow' electrons to the reduction of O_2 and H^+. PTOX enables continued functioning of PSII in generating a charge separation and driving H_2O oxidation, while at the same time limiting photodamage.

Future challenges in optimizing photosynthetic outputs will likely be facilitated by elucidating the regulation of enzymes involved in both sustainable and non-sustainable photochemical quenching. The information generated can be exploited to develop platforms for engineering the energetics of plants for better satisfying global food and resource needs.

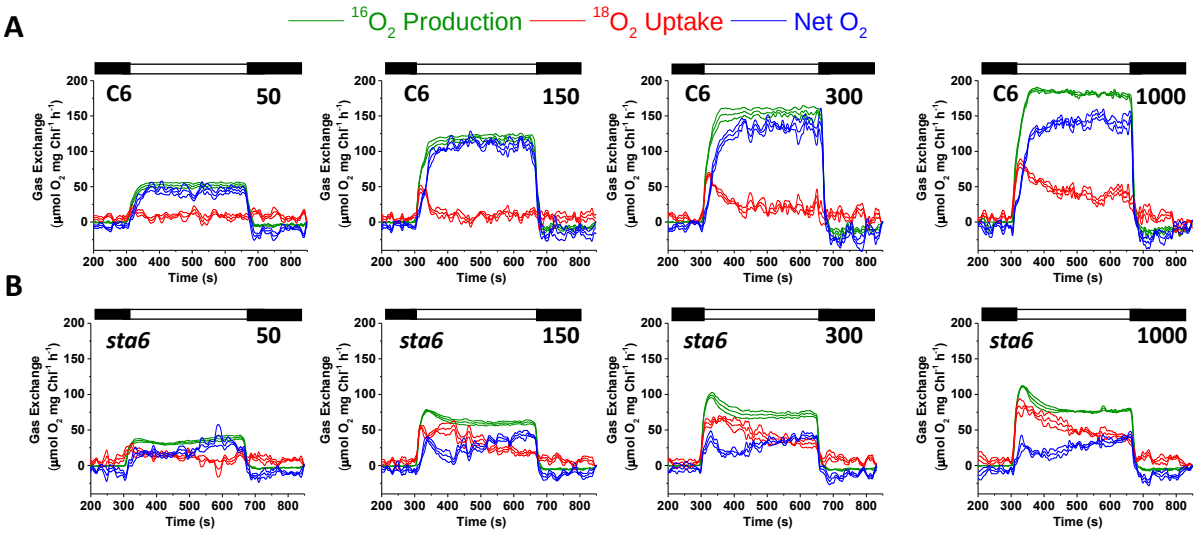

Figure 1: Light-induced O_2 evolution and uptake. C6 (**A**) and *sta6* (**B**) were cultured photoautotrophically, bubbled with 2 % CO_2 in air and maintained in continuous light of 100 µmol photons m^{-2} s^{-1}. Gross O_2 production ($^{16}O_2$ evolution, green curve) and light-induced uptake of O_2 ($^{18}O_2$ uptake, red curve) were monitored for 6 min using MIMS at 4 different light intensities (50, 150, 300 and 1000 µmol photons m^{-2} s^{-1}, as indicated in the figure). Prior to turning on the light, the cells were maintained for 5 min in the dark (black bars on the left of each graph), and for an additional 3 min in the dark following the illumination (black bar, on the right of each graph). Gross O_2 uptake and both gross and net (blue curve) O_2 production were calculated according to the formula given in Materials and Methods. Each trace represents an average of at least 3 biological replicates.

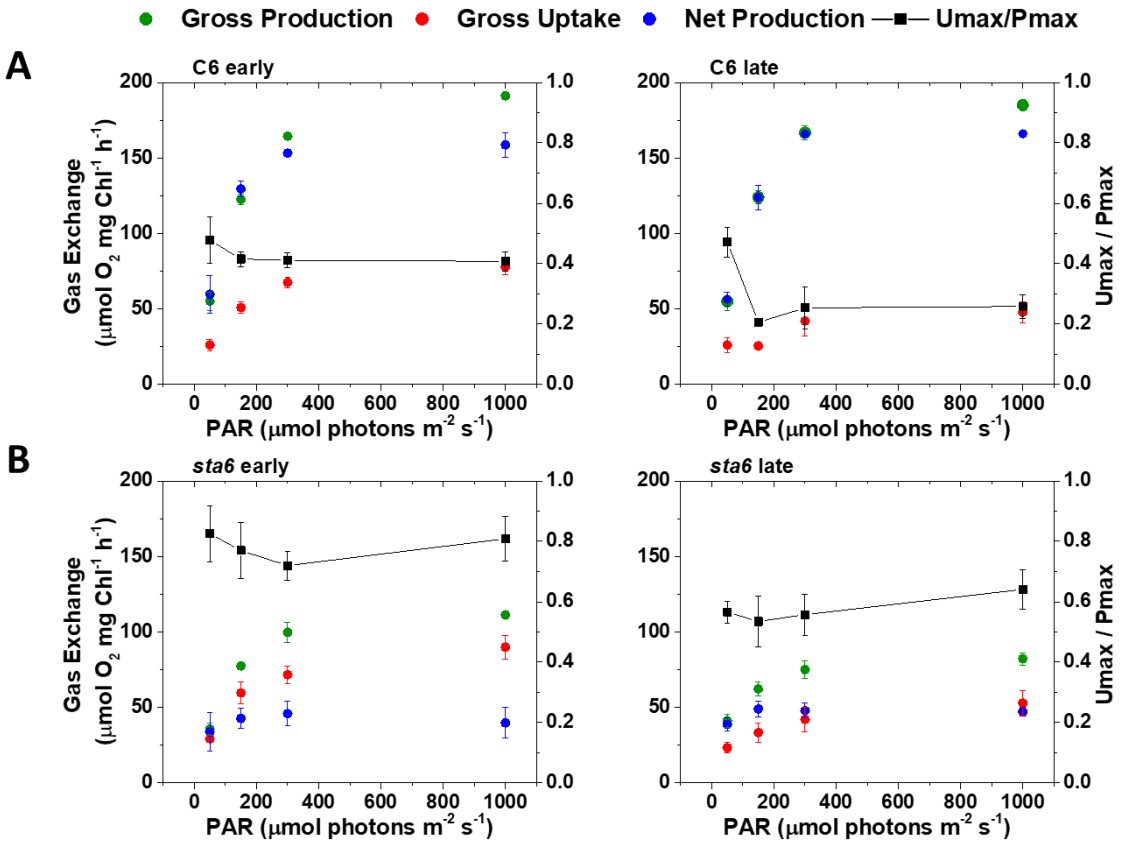

Figure 2: Maximal rates of light-induced O_2 production and uptake. Maximal values for gross and net O_2 production (green and blue, respectively) and gross O_2 uptake (red) for C6 (**A**) and *sta6* (**B**), are plotted as a function of light intensity. The left-hand Y-axis gives gross and net O_2 evolution and gross O_2 uptake, as indicated on the top of the figure. The right-hand Y-axis gives the ratio of maximal gross O_2 uptake relative to maximal gross O_2 production; this value is plotted as a function of light intensity (black line with black squares). For both **A** and **B**, the left panel presents the data for the first 3 min of the light phase while the right panel present the data for the final 3 min of the light phase (i.e. early and late periods during illumination, respectively; see main text for details). Net O_2 evolution was calculated as gross O_2 production – gross O_2 uptake. Each point is an average of at least 3 biological replicates ± SD.

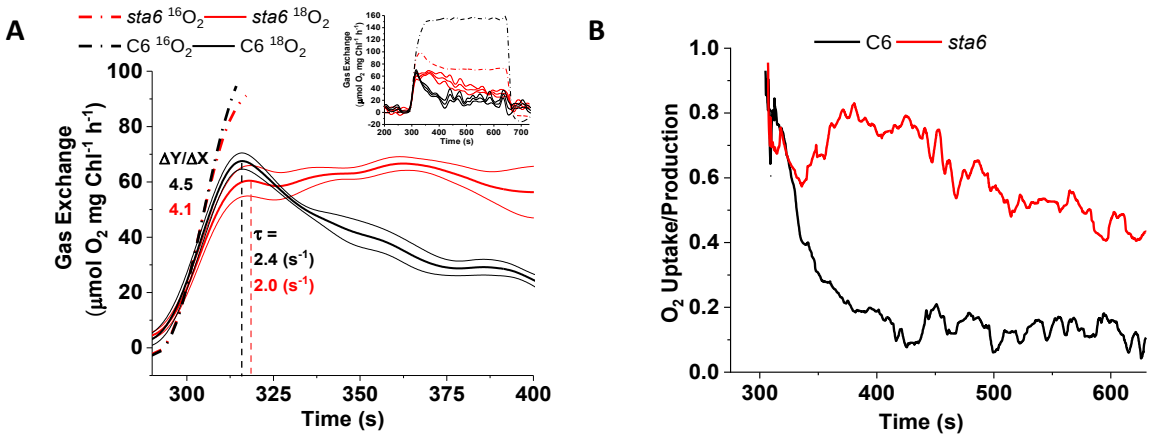

Figure 3: Kinetics of light-induced O_2 production and uptake. **A**. MIMS traces of $^{16}O_2$ evolution (gross production, dotted-dashed lines) and $^{18}O_2$ uptake (gross uptake, solid lines) during dark to light transition (300 µmol photons m^{-2} s^{-1}) for C6 (black) and *sta6* (red). Gross O_2 production ($^{16}O_2$) data during the first 20 s of the light period was linearly fitted and the initial rates ($\Delta Y/\Delta X$) calculated (black and red dash-dotted lines). $^{18}O_2$ uptake curves were fitted to a first-order exponential decay curves to determine the rate (τ) at which a peak of $^{18}O_2$ uptake for C6 and *sta6* were attained (dashed black and red line for C6 and *sta6*, respectively). **Inset**: Presentation of the MIMS traces for gross O_2 evolution and uptake during the entire light period (SE is only shown for gross O_2 uptake). **B**. The ratio between gross $^{18}O_2$ uptake and $^{16}O_2$ production during the light period (300 µmol photons m^{-2} s^{-1}). Same conditions as in panel **A**. Gray box highlights the region in which the decline in the ratio for C6 and *sta6* cells is similar. Each data line represents an average of 3 biological replicates.

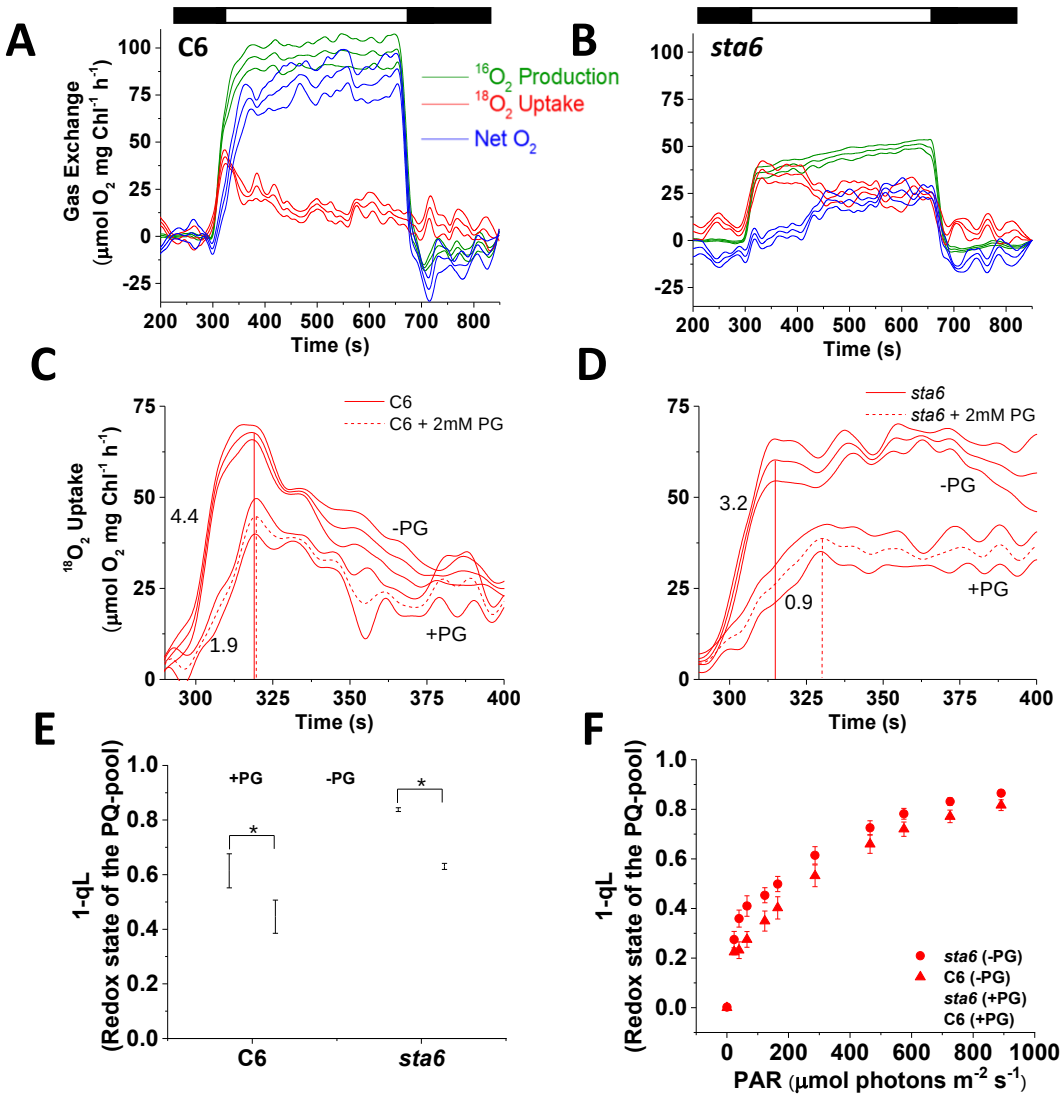

Figure 4: Effect of a PTOX on O_2 production and light-induced O_2 uptake. C6 (**A**) and *sta6* (**B**) were exposed to 300 µmol photons m^{-2} s^{-1} (white bars) in the presence of 2 mM propyl gallate (PG) and gas exchange was analyzed using MIMS, as in **Figure 3** (see **Figure 3** legend). Comparisons of the first 2 min of $^{18}O_2$ uptake for C6 (**C**) and *sta6* (**D**) in the presence (dashed line with purple shading) and absence (solid line with red shading) of PG. The time (s) to achieve Umax for C6 and *sta6* are highlighted by dotted red lines that extend from the X-axis to the Umax peak. Each trace represents an average of at least 3 biological replicates with the shaded area associated with each trace representing the SE. (**E**) 1-qL values of PG-treated/untreated cells. The cells were PG treated during the 5 min pre-incubation in the dark and then exposed to 300 µmol photons m^{-2} s^{-1} for 1 min. N=3 ±SD * t-test, *p-value* = 0.01. (**F**) 1-qL values of PG-treated/untreated cells exposed to increasing light intensities. Cells were exposed to each intensity for 30 s before raising the intensity. N=3 ±SD. PAR = photosynthetic active radiation.

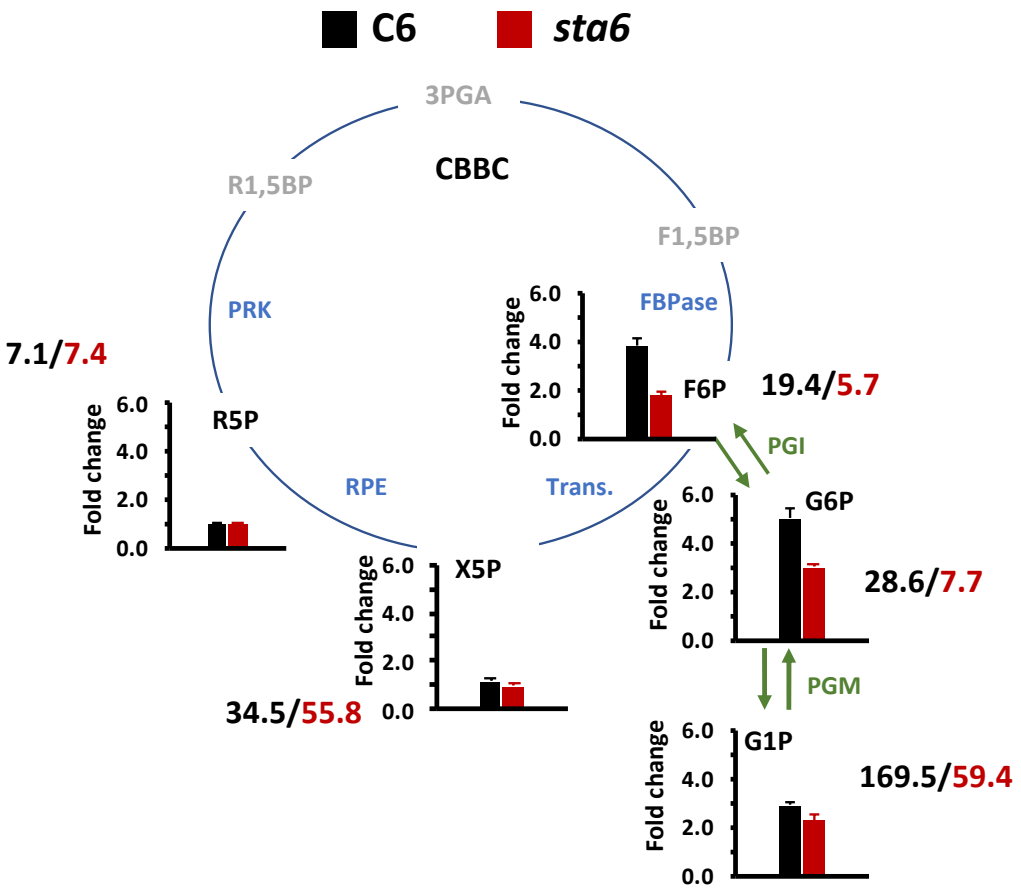

Figure 5: Conversion of F6P to CBBC and starch synthesis pathways: Metabolite profiling following exposure of C6 and *sta6* cells (black and red bars respectively) to light for 60 s. Starch biosynthesis pathway is highlighted in green, while CBBC is highlighted. Metabolites are shown in black. The numbers next to each metabolite represent the concentration of the metabolite following 60 s exposure to light in ng/10^7 cell. Each bar graph represents 4-6 biological replicates ± SE. Abbreviations: Metabolites: F6P- fructose 6-phosphate; G6P-glucose 6-phosphate; G1P- glucose 1-phosphate; X5P- Xylulose 5-phosphate; R5P-Ribulose 5-phosphate; R1,5,BP - Ribulose 1,5- bisphosphate; 3PGA- 3-phosphglyceraldehyde; F1,5BP-fructose 1,6- bisphosphate. Enzymes: PGI - phosphoflucoisomerase; PGM - phosphoglucomutase; Trans. - transaldolase; RPE – Ribulose –phosphate 3-epimerase

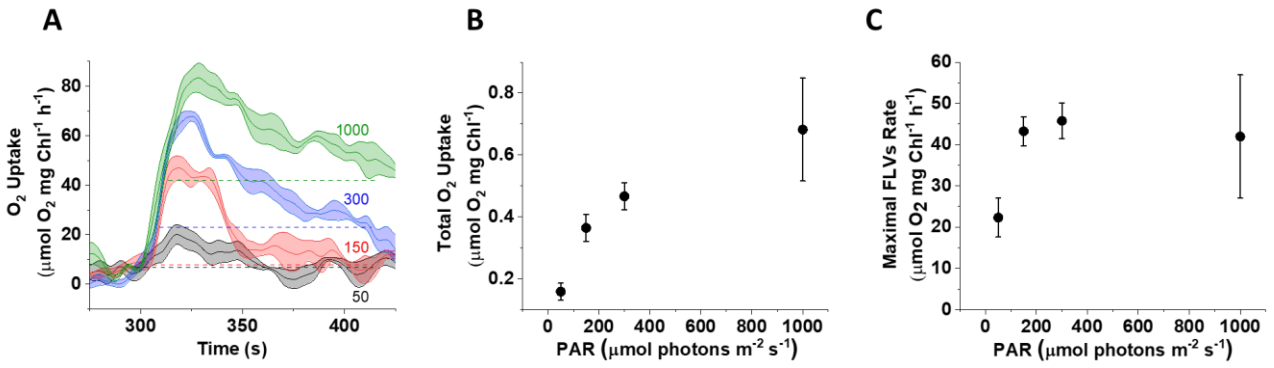

Figure 6: O_2 Uptake attributed to FLV proteins: **A**. O_2 uptake rate of C6 cells exposed to different light intensities (shown in different colors and indicated on the graph) are plotted during the first 2 min of the light period (300 - 420 s). The rates of baseline O_2 uptake (uptake in the light after the CBBC becomes active), calculated from **Figure S3**, are shown as dashed lines in the color that corresponds to the measurements of total O_2 uptake. **B.** Total O_2 uptake at each intensity that cannot be attributed to the basal rate of uptake was calculated by integrating the area between the curve defining the uptake rate at the different intensities with the rate of basal uptake at that intensity. **C.** Maximal rate of O_2 uptake attributed to the FLV proteins. These values were calculated by subtracting the rate of O_2 uptake attributed to basal uptake from Umax depicted in the curve in **A**. For all panels N=3 ± SD.

CRISPR/Cas9 disruption of glucan synthase in Nannochloropsis gaditana attenuates accumulation of β-1,3-glucose oligomers

These efforts were directed at studying alternative electron transport pathways in a marine alga that is a model system for lipid biofuels. The blocking of starch should increase lipid yields if photosynthetic activity is maintained.

Nannochloropsis species have garnered significant interest for biofuel production due to their ability to accumulate high levels of triacylglycerols (TAGs), especially following nitrogen-starvation. However, the first response to nutrient starvation is the synthesis of laminarin, a soluble β-1,3-glucan with β-1,6-branching. We employ CRISPR/Cas9 to knock out two key enzymes responsible for the polymerization of the oligosaccharide: a beta-glucan synthase (BGS) gene putatively responsible for the glucose β-1,3-linkage, and a transglycosylase (TGS) which putatively catalyzes the β-1,6-branching. The biosynthetic genes were knocked out in a mutant line of *Nannochloropsis gaditana* CCMP526 with stable Cas9 transgenic expression. This line was subsequently transformed with single guide RNAs (sgRNAs) targeting the genes of interest, into which antibiotic selection markers were inserted. This technique was demonstrated to be highly effective, with desired insertional mutagenesis observed in ~50% of the transformed lines. Analysis of the biomass from the generated mutants confirmed a significant decrease in accumulation of the soluble carbohydrate following nitrogen starvation.
Upon transfer to nitrogen-deficient media, wild-type and Cas9-GFP expressing cell lines accumulated significant methanol insoluble-water soluble (MIWS) carbohydrate. Relative to cultures maintained in nitrogen-replete media, MIWS carbohydrate increased per cell and as a fraction of dry cell weight (%DCW) 4-fold (Figure 1).

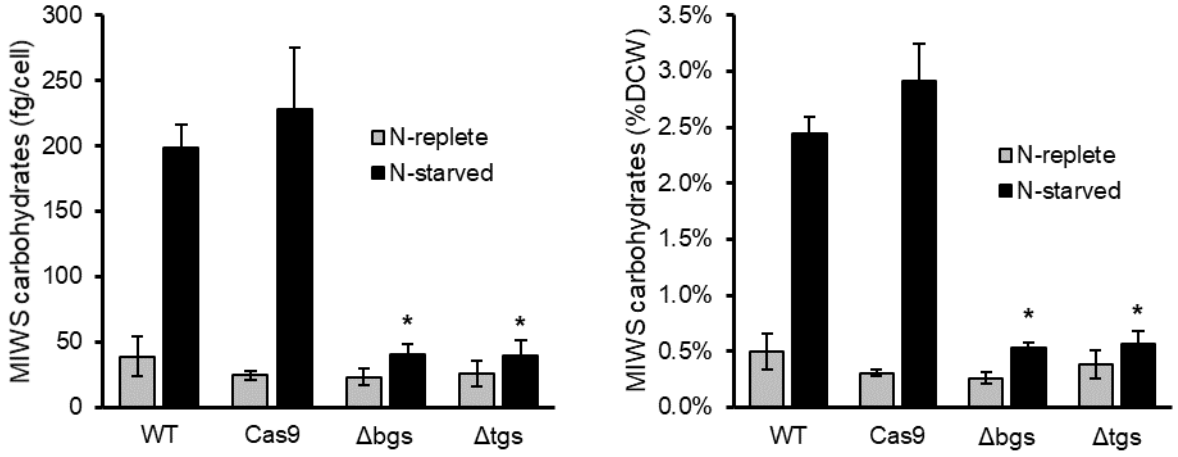

Figure 1. MIWS carbohydrate extracted from cultures split into nitrogen replete and nitrogen starved media at late exponential phase and cultured for 72 h. Error bars represent standard deviations of biological triplicates. MIWS carbohydrate is presented on a per cell (left) and fraction of dry cell weight (right) basis. Asterisks (*) indicate significant difference from both wild-type and Cas9-GFP background (p-value < 0.05).

Knockout of BGS or TGS drastically reduces MIWS carbohydrate accumulation

In both sets of knockouts, MIWS carbohydrate was significantly reduced relative to both wild-type and Cas9-GFP-expressing cultures following nitrogen starvation. The effect was not

noticeable in nitrogen replete conditions, but following nitrogen starvation, carbohydrate levels were comparable to nitrogen-replete control cultures for the two mutants (Figure 1).

It is surprising that the Δ*tgs* line displayed a similar disruption of MIWS carbohydrate accumulation. One likely explanation is the formation of an enzyme complex which does not form or function properly in the absence of the branching enzyme. Another explanation might be that the lack of beta glucan branching causes the storage carbohydrate to be less soluble, causing its loss from the analyzed MIWS fraction. To investigate this possibility, we also quantified the total carbohydrate from these same cultures (Figure 2).

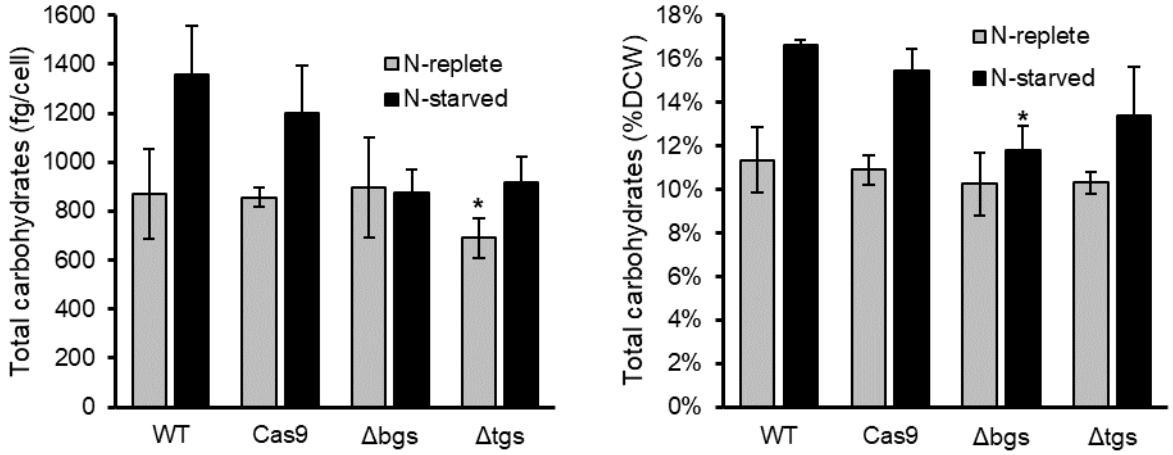

Figure 2. Total carbohydrate from cultures split into nitrogen replete and nitrogen starved media cultured for 72 h to late exponential phase. Error bars represent standard deviations of biological triplicates. Carbohydrate is presented on a per cell (left) and fraction of dry cell weight (right) basis. Asterisks (*) indicate significant difference from both wild-type and Cas9-GFP background (p-value < 0.05).

We did not observe a corresponding decrease in total carbohydrate for the Δ*tgs* line in nitrogen-starved conditions on a dry cell weight basis. However, a decrease was observed in nitrogen-replete conditions on a per cell basis. It may be that the lack of branching effects the capacity to store the carbohydrate, perhaps effecting packing efficiency. Alternatively, it may be that the branch sites function to regulate the breakdown of this storage carbohydrate, and that branching is one mechanism to moderate the degradation and use of the carbohydrate.

It should also be pointed out that the understanding of the β-1,6-transglycosylase is very limited. Almost all of our knowledge comes from inference by homology to the yeast Kre6 proteins, believed to be involved in the β-1,6-branching of β-1,3 chains of yeast cell walls [20,21]. The capacity for *tgs* genes of *P. tricornutum* to functionally complement a transglycosylase-deficient Δ*kre6* yeast strain supports the functional similarity of these two genes [22]. In *C. albicans*, knockdown of *skn1* (the conserved domain present in the *tgs* genes of stramenopiles) reduced β-1,6-glucan with no effect on β-1,3-glucan [21], but in *Saccharomyces cerevisiae*, mutations of *KRE6* reduced levels of both β-1,6-glucan and β-1,3-glucan [23].

3.3. Growth under light/dark cycling

In *P. tricornutum*, *bgs* knockdowns demonstrated a lower growth rate than wild-type under constant light, but differential growth was lost in light/dark cycles with short days (8L/16D, 4L/20D [6]. In our growth experiments under light/dark cycling (Figure 3), both knockouts grew similarly to the Cas9-expressing background line (Figure 3).

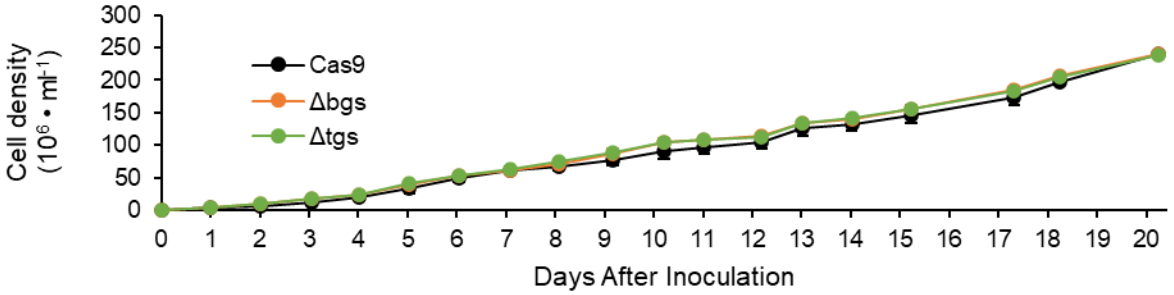

Figure 3. Cell densities over time. No significant difference in growth is observable between the selected strains. Error bars represent standard deviation of four biological replicates, except for wild-type. For each knockout, four genetically unique mutants were used.

3.4. BGS knockout strains accumulate significantly more lipids

In diatom knockdowns of the beta glucan synthase, total fatty acid accumulation was increased relative to wild-type [6,24]. Within *T. pseudonana*, an array of knockdowns with unmeasured effect on transcript or protein levels yielded greater total fatty acid accumulation only at stationary phase of culture [24]. A knockdown in *P. tricornutum* yielded a near doubling of total fatty acid content relative to WT following nitrogen depletion. While we did notice an ~25-40% increase in total fatty acid content under replete conditions ($p < 0.01$, Figure 4), the increase was not statistically significant following nitrogen starvation ($p > 0.05$).

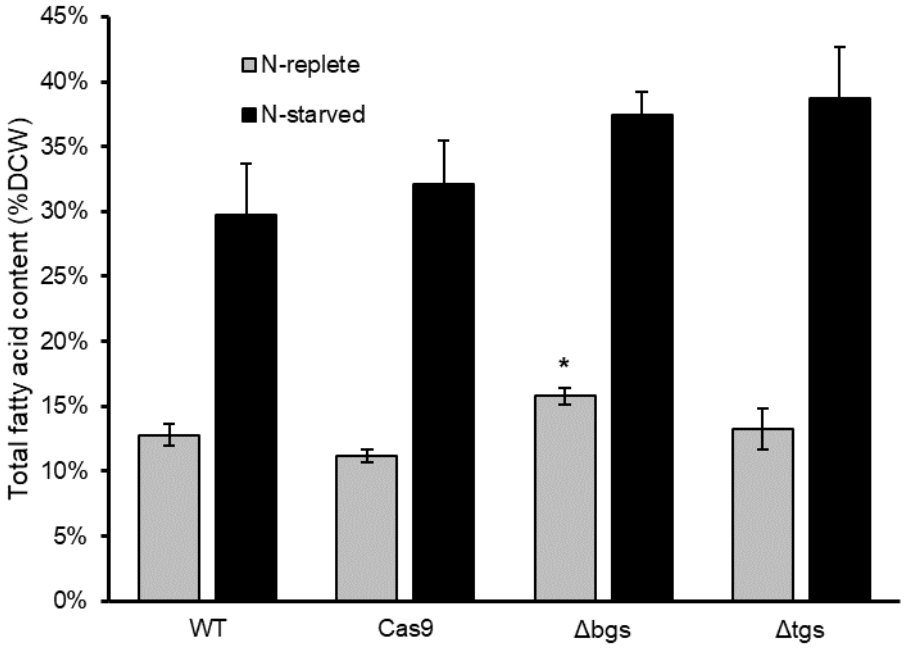

Figure 4. The total fatty acid content as a fraction of dry cell weight (%DCW) for cultures split into nitrogen replete and nitrogen starved media at late exponential phase and cultured for 72 h. Error bars represent standard deviations of biological triplicates. Asterisk (*) indicates statistically significant difference from both wild-type (WT) and Cas9-GFP background ($p < 0.01$).

BGS disrupted cells maintain high chlorophyll in older cultures

Interestingly, we observed a unique phenomenon in Δ*bgs* mutant lines after ten days of diel culturing, at densities above 1×10^8 cells/ml. At this late growth stage, the Cas9 background and the Δ*tgs* mutants exhibit a shift in autofluorescence, fluorescing less at 695 nm (chlorophyll autofluorescence) and more at 574 nm (referred to here as carotenoid autofluorescence [25]) (Fig. 5, top). There appear to be three discrete subpopulations: a typical population present throughout growth of all cultures with high chlorophyll autofluorescence and low carotenoid fluorescence (high Chl), a transitionary population with reduced chlorophyll autofluorescence and increased carotenoid fluorescence (mid Chl), and a population with further reduced chlorophyll autofluorescence and increased carotenoid fluorescence (low Chl). In the Δ*bgs* knockout lines, the transition appeared significantly later, and the low Chl subpopulation remained significantly smaller than that observed for either the Cas9 or the Δ*tgs* knockout lines (Fig. 5, bottom).

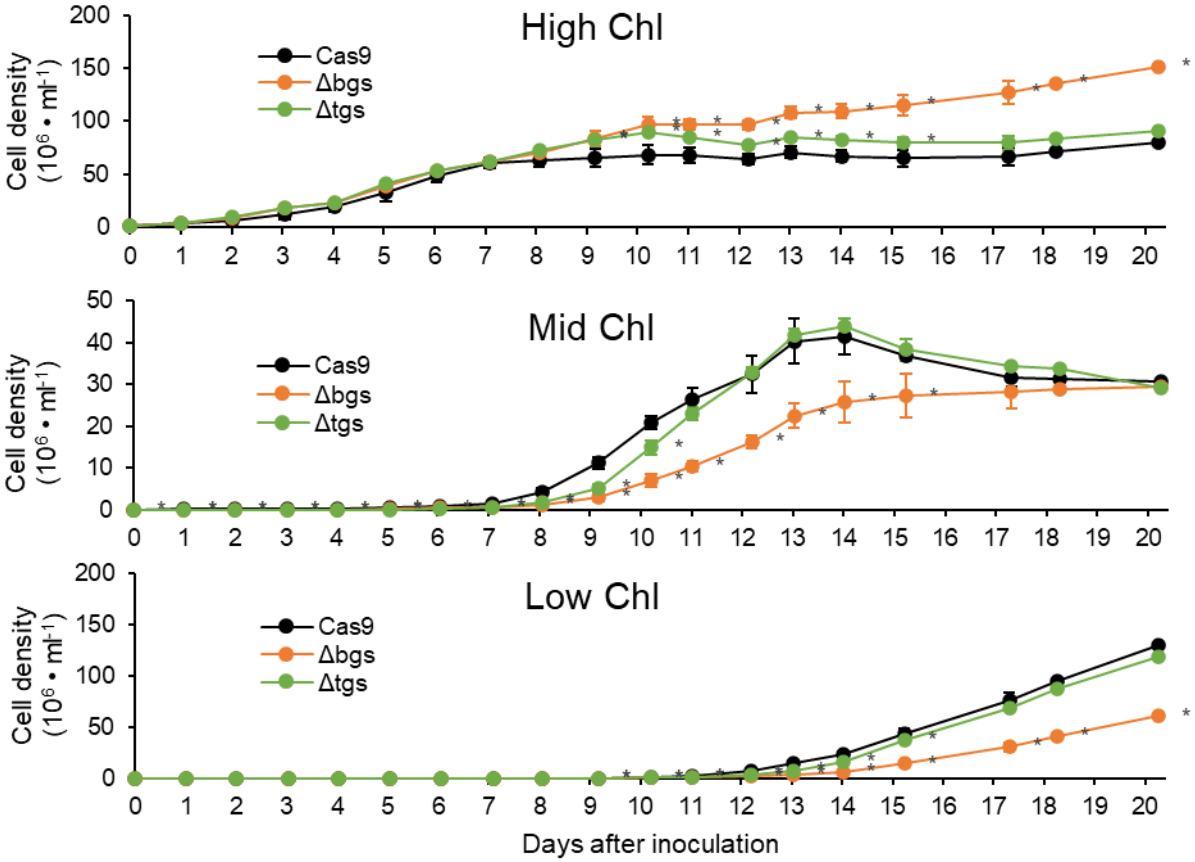

Figure 5. Subpopulations with discrete fluorescence profiles at 20 days (top). Cells are excited by 488 nm laser and emissions at 695 nm (chlorophyll autofluorescence) and 574 nm (carotenoid autofluorescence) are measured for each event. Shown are flow cytometry scatterplots of one representative sample from each group at day 20. Cell densities of fluorescent subpopulations are measured as cultures mature (bottom). In exponential growth, nearly all cells exhibit high chlorophyll autofluorescence (high Chl). As cultures mature, a population appears with reduced 695 nm fluorescence and increased 574 nm fluorescence (mid Chl). Later, a population with further reduced 695 nm fluorescence and increased 574 nm fluorescence appears (low Chl) and the transitional population fades. Error bars represent standard deviation of four biological replicates. For knockouts, four genetically unique mutants were used. Asterisks (*) indicate significant difference from Cas9-GFP background (p-value < 0.05).

These results suggest a role for the storage glucan in regulating the operation of light harvesting and energy transfer. We investigated whether this shift in autofluorescence correlates to a difference in chlorophyll or carotenoid content. In our Δ*bgs* knockout lines, we observe more chlorophyll and carotenoids per cell relative to both the Cas9-GFP background and Δ*tgs* knockout lines (Figure 6). We did not observe a significant difference in the ratio of carotenoids to chlorophyll. We did not examine the structure of the plastid, which was altered significantly in the diatom *bgs* knockdown [6].

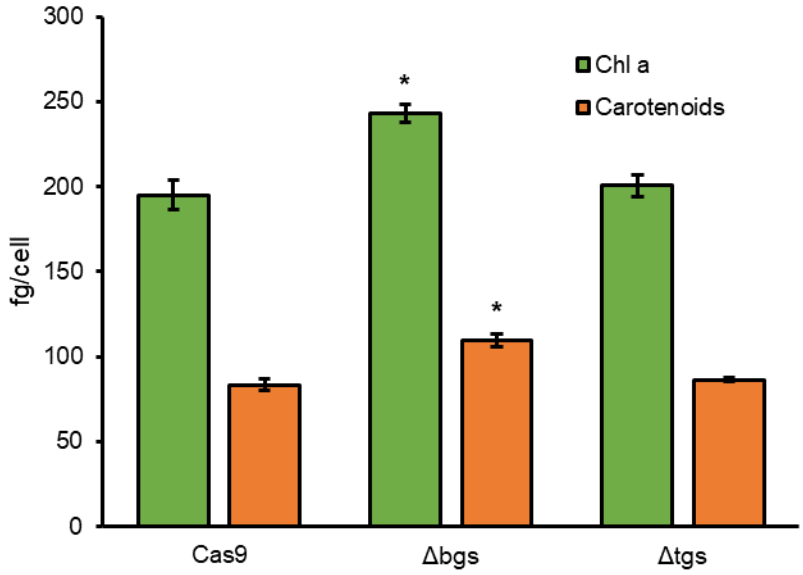

Figure 6. Chlorophyll a and carotenoid content of late exponential phase cultures (1.2-1.5x10^8 cells/ml) grown under 12/12 light/dark cycle. Samples were taken at 8 hrs into the 12 hr light period. Error bars represent standard deviation of four biological replicates. For knockouts, four genetically unique mutants were used. Asterisks (*) indicate significant difference from Cas9-GFP background (*p*-value < 0.05).

Knockout of the predicted beta-glucan synthase gene in *Nannochlorpsis gaditana* confirms its essential involvement in the synthesis of the β-1,3-linked soluble storage carbohydrate by significantly reducing its accumulation. Suprisingly, knockout of the predicted branching enzyme had a similar effect, also significantly reducing levels of the storage carbohydrate.
We demonstrated a modest increase in lipid levels under nutrient-replete conditions relative to wild-type and Cas9-expressing background. We did not observe the growth defects shown by knockdowns of the beta-glucan synthase gene in *Phaeodactylum tricornutum*, instead the deletion lines grow just as well under both constant light and a light/dark cycle.Storage carbohydrates have been observed to mediate stress response in cyanobacteria [26] and plastid organisation in diatoms [6]. In this work, we observe significant changes to cell autofluorescence resulting from the knockout of the beta-glucan synthase.

Critical role of *Chlamydomonas reinhardtii* ferredoxin-5 in maintaining membrane structure and dark metabolism

Yang, W., Wittkopp, T.M., Li, X., Warakanont, J., Dubini, A., Catalanotti, C., Kim, R.G., Nowack, E.C.M., Mackinder, L., Aksoy, M., Page, M.D., D'Adamo, S., Saroussi, S., Heinnickel, M., Johnson, X., Richaud, P., Alric, J., Boehm, M., Jonikas, M.C., Benning, C., Merchant, S.S., **Posewitz, M.C.**, and Grossman, A.R. (2015) Critical role of *Chlamydomonas reinhardtii* ferredoxin-5 in maintaining membrane structure and dark metabolism. *Proceedings of the National Academy of Sciences* USA, **12**, 14978-14983. doi: 10.1073/pnas.1515240112.

Photosynthetic microorganisms typically have multiple isoforms of the electron transfer protein ferredoxin, although we know little about their exact functions. Surprisingly, a *Chlamydomonas reinhardtii* mutant null for the ferredoxin-5 gene (*FDX5*) completely ceased to grow in the dark, with both photosynthetic and respiratory functions severely compromised; whereas growth in the light was unaffected. Thylakoid membranes in dark-maintained *fdx5* mutant cells became severely disorganized concomitant with a marked decrease in the monogalactosyldiacylglycerol (MGDG) to digalactosyldiacylglycerol ratio, two dominant lipids in the photosynthetic membranes, and accumulation of triacylglycerol. Furthermore, FDX5 directly interacts with the fatty acid desaturases CrΔ4FAD and CrFAD6, likely donating electrons for the formation of desaturated fatty acids that stabilize MGDG. The mutant's inability to grow in the dark may be a consequence of the role of FDX5 in fatty acid oxidation and maintaining proper membrane lipid composition, or another critical dark, FDX5-dependent activity. Alternative electron carriers must assume the role of FDX5 in the light. Our results clearly establish that in photosynthetic organisms, specific electron mediators sustain dark metabolism, with little impact on day-time growth, likely reflecting the tailoring of electron carriers to unique intracellular metabolic circuits under these two very distinct redox conditions.

Summary

The overarching purpose of the research was to define and map electronic transfer circuits in eukaryotic with an emphasis on the model system *Chlamydomonas reinhardtii*, but also integrating emerging algal systems to better understand the conservation of these circuits. Early research focused on the dark phase of energy management and how metabolic circuits adapt to blocks in primary fermentation pathways. These efforts demonstrated that algae are extremely metabolically versatile organisms that can readily activate alternative pathways for the generation of cellular ATP and survival. Importantly, many of the products are (e.g. lactate, succinate, glycerol, hydrogen, ethanol) are of biotechnological value for use as fuels and commodity bioproducts. Later efforts focused on alternative circuits activated in the light when dominant carbon sinks are blocked (e.g proteins, carbohydrates). These efforts are focused on understanding how excitation energy is managed when carbon is not routed to the primary endpoints. The research revealed and quantified the activation of O_2-reduction pathways that compete with carbon fixation for low-potential electrons. Additionally, a reversible switch was identified under extreme conditions that prevent electrons from damaging photosystem I when carbon fixation is blocked. These efforts provide the framework to engineer electron transfer to lipid biosynthetic pathways and to maintain photosynthetic activity and carbon fixation when primary carbon assimilation routes are disrupted.

Accepted Publications

1. Saroussi, S., Karns, D.A.J., Thomas, D.C., Bloszies, C., Fiehn, O., **Posewitz, M.C.** and Grossman, A.R. (2019) Alternative outlets for sustaining photosynthetic electron transport during dark to light transitions. *Proceedings National Academy of Sciences*, **116**, 11518-11527.
2. **Posewitz, M.C.** (2018) Metabolism and genetics of algal hydrogen production. In Microalgal Hydrogen Production: Achievements and Perspectives. Seibert M. and Torzillo G. Eds. Royal Society of Chemistry, Cambridge. Chapter 7, pages 167-188.
3. Gu, H., Jinkerson, R.E, Davies, F.K., and **Posewitz, M.C.** (2016) Modulation of Medium-Chain Fatty Acid Synthesis in *Synechococcus* sp. PCC 7002 by Replacing FabH with a *Chaetoceros* Type III ketoacyl-ACP synthase. *Frontiers in Lipid Research*, doi: 10.3389/fpls.2016.00690.
4. Yang, W., Wittkopp, T.M., Li, X., Warakanont, J., Dubini, A., Catalanotti, C., Kim, R.G., Nowack, E.C.M., Mackinder, L., Aksoy, M., Page, M.D., D'Adamo, S., Saroussi, S., Heinnickel, M., Johnson, X., Richaud, P., Alric, J., Boehm, M., Jonikas, M.C., Benning, C., Merchant, S.S., **Posewitz, M.C.**, and Grossman, A.R. (2015) Critical role of *Chlamydomonas reinhardtii* ferredoxin-5 in maintaining membrane structure and dark metabolism. *Proceedings of the National Academy of Sciences* USA, **12**, 14978-14983. doi: 10.1073/pnas.1515240112.
5. Yang, W., Catalanotti, C., Wittkopp, T.M., **Posewitz, M.C.** and Grossman, A.R. (2015) Algae after dark: mechanisms to cope with hypoxia/anoxia. *Plant Journal* **82**, 481-503. doi: 10.1111/tpj.12823.
6. Davies, F.K., Jinkerson, R. J., and **Posewitz, M.C.** (2015) Toward a photosynthetic microbial platform for terpenoid engineering. *Photosynthetic Research* **123**, 265-284.
7. Yang, W., Catalanotti, C., D'Adamo, S., Wittkopp, T.M., Ingram-Smith, C.J., Mackinder, L., Miller, T.E., Heuberger, A.L., Peers, G., Smith, K.S., Jonikas, M.C., Grossman, A.R. and **Posewitz, M.C.** (2014) Alternative acetate production pathways in *Chlamydomonas reinhardtii* during dark anoxia and the dominant role of chloroplasts in fermentative acetate production. *Plant Cell* **26**, 4499-4518.
8. Yang, W., Catalanotti, C., **Posewitz, M.C.**, Alric, J., and Grossman, A.R. (2014) Insights into algal fermentation. In: Low-Oxygen Stress in Plants; Plant Cell Monographs, Vol. 2. J.T, van Dongen and F. Licausi (Eds.), Springer, Dordrecht, Netherlands, pp. 135-163.
9. Catalanotti, C., Yang, W., **Posewitz, M.C.** and Grossman, A.R. (2013) Fermentation metabolism and its evolution in algae. *Frontiers in Plant Science* **4**, 150, 1-17.
10. Catalanotti, C., Dubini, A., Subramanian, V., Yang, W., Magneschi, L., Mus F., Michael Seibert, M., **Posewitz, M.C.** and Grossman, A.R. (2012) Altered fermentative metabolisms in *Chlamydomonas reinhardtii* mutants lacking PFL1 and both PFL1 and ADH1. *Plant Cell* **24**, 692-707.
11. Magneschi, L., Catalanotti, C., Subramanian, V., Dubini, A., Yang, W., **Posewitz, M.C.**, Seibert, M., Perata, P., and Grossman A.R. (2012) A mutant in *ADH1* of *Chlamydomonas reinhardtii* elicits metabolic restructuring during anaerobiosis. *Plant Physiology* **158**, 1293-1305.
12. Meuser, J.E., D'Adamo, S., Jinkerson, R.E., Mus, R., Yang, W., Ghirardi, M.L., Seibert, M., Grossman, A.R., and **Posewitz. M.C.** (2012) Genetic disruption of both *Chlamydomonas reinhardtii* [FeFe]-hydrogenases: insight into the role of HYDA2 in H_2 production. *Biochemical and Biophysical Research Communications* **417**, 704-709.